SCIENTIFIC REPORTS

OPEN

SUBJECT AREAS:
ELECTRONIC DEVICES
NANOSCALE DEVICES

Received
23 September 2014

Accepted
15 December 2014

Published
19 January 2015

Correspondence and requests for materials should be addressed to C.S.H. (cheolsh@snu.ac.kr)

Dual Conical Conducting Filament Model in Resistance Switching TiO_2 Thin Films

Kyung Min Kim[1], Tae Hyung Park[2] & Cheol Seong Hwang[2]

[1]Hewlett-Packard Laboratories, Hewlett-Packard Company, Palo Alto, California 94304, USA, [2]Department of Materials Science and Engineering and Inter-university Semiconductor Research Center, Seoul National University, Seoul 151-744, South Korea.

The resetting behaviors of Pt/TiO_2/Pt resistive switching (RS) cell in unipolar RS operations were studied in detail through an experiment and by modeling. The experiment showed that the apparently highly arbitrary resetting current-voltage (I–V) curves could be grouped into three types: normal, delayed, and abnormal behaviors. A dual conical conducting filament (CF) model was conceived, and their electrothermal behaviors were analytically described from the heat-balance and charge-transport equations. The almost spontaneous resetting behavior of the normal reset could be easily understood from the mutually constructive interference effect between the Joule heating and temperature-dependent resistance effect along the CF. The delayed reset could be explained by the time-dependent increase in the reset voltage during the rest process, which was most probably induced in the more conical-shaped CF. The abnormal reset could be understood from the temporal transfer of oxygen ions near the kink positions of the two different-diameter portions of the more cylindrical CFs, which temporally decreases the overall resistance immediately prior for the actual reset to occur. The accuracy of the dual conical CF model was further confirmed by adopting a more thorough electrothermal simulation package, COMSOL.

The resistance switching (RS) behavior shown in various materials attracts a great deal of attention due to its high potential for the non-volatile memory, analog memristor, and neuromorphic applications[1–3]. Among the several switching mechanisms suggested for the diverse RS materials and devices[4–6], the formation and rupture of the conducting channel, which is normally called "conducting filament (CF)", is well accepted as the feasible RS mechanism in many transition metal oxides in the research field[5]. Since the systematic studies on the RS in the TiO_2 thin film conducted by Christina et al[7]. and Choi et al.[8], TiO_2 has been regarded as the most representative material showing the filamentary RS. The major achievements in understanding the precise RS mechanism in TiO_2 have been made by Kim et al.[9–12], who suggested the anode interface localized switching induced in the conical CF, and by Kwon et al.[13], who identified the Magnéli phase (Ti_nO_{2n-1}), such as Ti_4O_7 and Ti_5O_9, as the main constituent of the CFs via high-resolution transmission electron microscopy. The need to form the conical filament shape can be explained by the nucleation and growth behavior of the filaments[5]. The oxygen vacancy begins to be generated at the cathode interface due to the localized Joule heating caused by the majority carrier injection, which assists the drift of the oxygen ions. This corresponds to the filament nucleation step. Then the filament nuclei extend towards the anode interface and expand laterally at the later stage[14], which corresponds to the filament growth step. Consequently, the conical filament is formed with the filament being stronger at the cathode interface and weaker at the anode interface. Due to this asymmetry in the CF shape, only a 3–10 nm portion with weaker strength near the anode among the 40-nm-long CF was ruptured[10]. Subsequently, Kim et al.[15] and Kim et al.[16] showed that the shapes and physical locations of the CFs along the lateral and vertical directions of the thin film could be manipulated as desired. The critical ingredients of these reports were based on the fact that the Magnéli CF has an asymmetric shape (conical shape) along its lengthwise direction, which almost always induces localized rupture and rejuvenation near the anode interface[12,13]. The ruptured parts of the Magnéli CF play a crucial role in the subsequent bipolar resistance switching (BRS)[17] due to either the migration of the oxygen vacancies[18] or the trapping/detrapping of the electronic carriers[19–21].

The Magnéli-CF-involved RS mechanism is generally of a unipolar RS (URS) nature, where the thermal motion of the ions (or vacancies) due to the Joule heating effect plays a critical role. This is especially the case when reset switching (switching from the low-resistance state or LRS to the high-resistance state or HRS) occurs, whereas set switching (switching from HRS to LRS) is more electric-field-driven albeit also thermally assisted[5]. Therefore, the

important reset switching parameters, such as the reset voltage (V_{RES}) and the current (I_{RES}), can be closely related with the thermal behavior through the CF, the heat generation via the Joule heating effect, and the heat dissipation through the matrix phase, which are largely determined by the geometric shape of the CF as well as its physical parameters. Based on these ideas, the authors reported interesting variations in the V_{RES} according to the resistance of LRS (R_{LRS}), which represents the geometric configuration of the CF. An increase in the CF volume with increasing input set switching power (or compliance current, I_{CC}) was achieved while the overall conical shape was maintained when the CF diameter was small ($<\sim$10 nm)[12]. In contrast, when the CF diameter became larger, the conical shape changed to a more cylindrical one, making the CF more symmetrical along the lengthwise direction[12]. While it was not explicitly mentioned in that report, the more cylindrical shape of the CF could contribute to the more random fluctuation of the RS parameters because any part of the cylindrical CF could be ruptured. In fact, this has good correspondence with the general trend in TiO_2 wherein the lower the R_{LRS} is, the higher the fluctuations in the switching parameters[22]. The authors further progressed in understanding the correlation between the CF shape and the switching parameters, which was summarized in the report on the correlation between the reset current (I_{RES}) and $1/R_{LRS}$[23]. This model can encompass the physical implication of the random circuit breaker model, which has been used to explain the RS in NiO[24].

Considering the high potential of such thermochemical approach to precisely and quantitatively explain the RS behaviors in TiO_2, the approach can be further developed to explain the more detailed set processes. Especially, this model can be used to explain the large fluctuations in the current-voltage (I–V) sweep curves during the reset operation, as shown in this report. In fact, the large fluctuations in the I–V curves for the given memory cell has been one of the big hurdles that the RS memory has to overcome to become a viable memory device. There have been several reports on the possible origins of and solutions to this critical problem[25,26]. The present work can add a meaningful improvement in the understanding of such important topic, which will trigger clever ways of overcoming such problem in the future. The idea of the present work is based on what has already been reported[12], where the Magnéli CF in TiO_2 could have a more conical or cylindrical shape depending on its overall electrical conductivity (a higher conductivity or a larger diameter prefers the cylindrical shape, and vice versa), and thus, the ruptured part at the HRS could be either near the tip of the CF (conical case) or in the middle of it (cylindrical case). The latter case is more probable when considering the loss of heat through a metal electrode in contact with the CF (the middle portion could have a much higher chance of being heated up to a temperature sufficient to induce the CF rupture) while the former case could obviously be induced for a much more conical case because the current crowding into the narrowest part of the conical CF will obviously heat up that part.

Experimental Procedure

The $Pt/TiO_2/Pt$ samples that were used in the experiments were identical to the samples reported in Ref. 9–13. In short, 40-nm-thick TiO_2 films were deposited via atomic layer deposition on a 50-nm-thick $Pt/SiO_2/Si$ substrate at 250°C, which resulted in a partly crystallized film (mixture of amorphous, anatase, and brookite phases). Electron-beam-evaporated 50-nm-thick Pt top electrodes with a typical area of 100×100 μm² were fabricated via lift-off photolithography. The I–V curves were measured using a Hewlett-Packard 4145B semiconductor parameter analyzer at room temperature, with a bias step of 0.01 V, with the top electrode (TE) Pt being biased while the bottom electrode (BE) Pt being grounded. Thirty consecutive I–V sweeps were performed to achieve the various curves of RS behavior. Simulation of the temperature profiles for the differently shaped CFs (conical or cylindrical) was performed using the COMSOL software package.

Results and Discussion

After the electroforming of the pristine sample, the RS operations were performed using a certain memory cell with an I_{cc} of 0.03 A. Figure 1a shows the RS I–V curves of the sample, which were acquired repeatedly (30 times). As usual, the I–V curves showed largely varying I–V behaviors with apparently no correlations between them. A careful examination of each curve, however, especially the curve shapes near the V_{RES}, will show that the curves can be grouped into three classes, as shown in Figures 1b, c, and d. In Figure 1b, the so-called "normal reset curves" were collected, which were observed 10 times in 30 trials. In this case, the current decreased very abruptly at V_{RES}, which could be more evidently confirmed from the inset figure, where only 0.01–0.02 V was generally necessary to reach the HRS after the V_{RES} was applied. Such an abrupt reset is a characteristic feature of URS, where a partial rupture of the metallic Magnéli CF induces an even more serious current crowding effect, which in turn increases the Joule heating again at V_{RES}[27]. Therefore, the local temperature at the specific location of the CF, which is supposed to be ruptured, increases very fast at the moment of reset. As will be discussed later, however, the reset in URS is not a purely thermal effect but is still quite largely influenced by the electric-field-driven ion migration. Even before the actual CF rupture occurs, the I–V curves showed deviation from the Ohmic behavior near V_{RES} (lower current compared with the expected Ohmic current from the behavior at a lower voltage), which could also be understood from the increase in the resistance by the Joule heating. This is not always the case, however, as shown in Figure 1c and d. Figure 1c shows the so-called "delayed reset curves" that were collected, whose occurrence was 8 out of 30, where the gradual current decrease was observed to be over 0.03–0.07 V prior to the current drop to HRS. The inset more precisely shows the delayed reset behavior. Another interesting feature can be found from the remaining 12 I–V curves, as shown in Figure 1d, which are called "abnormal reset curves". In this case, the current immediately prior to the reset switching slightly increased compared with the normal reset curves, which can be more clearly seen in the inset figure in Figure 1d. As can be understood from the almost uniform distributions (10, 8, and 12 in 30 trials) of these three different types of reset behaviors, the chances of the occurrence of these three cases are almost identical. If the non-uniform reset behavior is just the output of statistical reset behavior of a bunch of filaments, the normal reset and the delayed reset curves may be explained by the sequential rupture of filaments. However, the abnormal reset curves can never be understood from such simple statistical reasoning, while the chance of emerging such events was equally probable as others.

To understand such features in reset switching, the following "dual conical" model for the CF, and its thermal motion, were considered. Figure 2a shows the schematic diagram of the dual conical filament model in this work. Here, the filament is divided into two parts: the retained filament (CF_1) and the ruptured filament (CF_2) after the reset switching. It has been well understood that during the reset process, CF_1 will not be ruptured because of its relatively higher strength while CF_2 will be ruptured, which is actually responsible for the reset switching. Therefore, during the subsequent set switching step, CF_2 would be rejuvenated. Each filament part has its own shape, with a radius at the cathode side of r_1 and r_2 and at the anode side of $a_1 \cdot r_1$ and $a_2 \cdot r_2$, where a_1 and a_2 are the ratio of the radius between the cathode side and the anode side, whose value is $0 < (a_1 \text{ and } a_2) < 1$. Such dual filament model is applicable to any filament shape, even the complicated ones, as shown in Figures 2b–d. As aforementioned, the CF shape could be more conical or cylindrical, as shown in the left and right parts of Figure 2b, depending on the electroforming conditions, and could have ruptured configurations after the reset switching, as shown in Figure 2c, which corresponds to CF_1 in each case. This is due

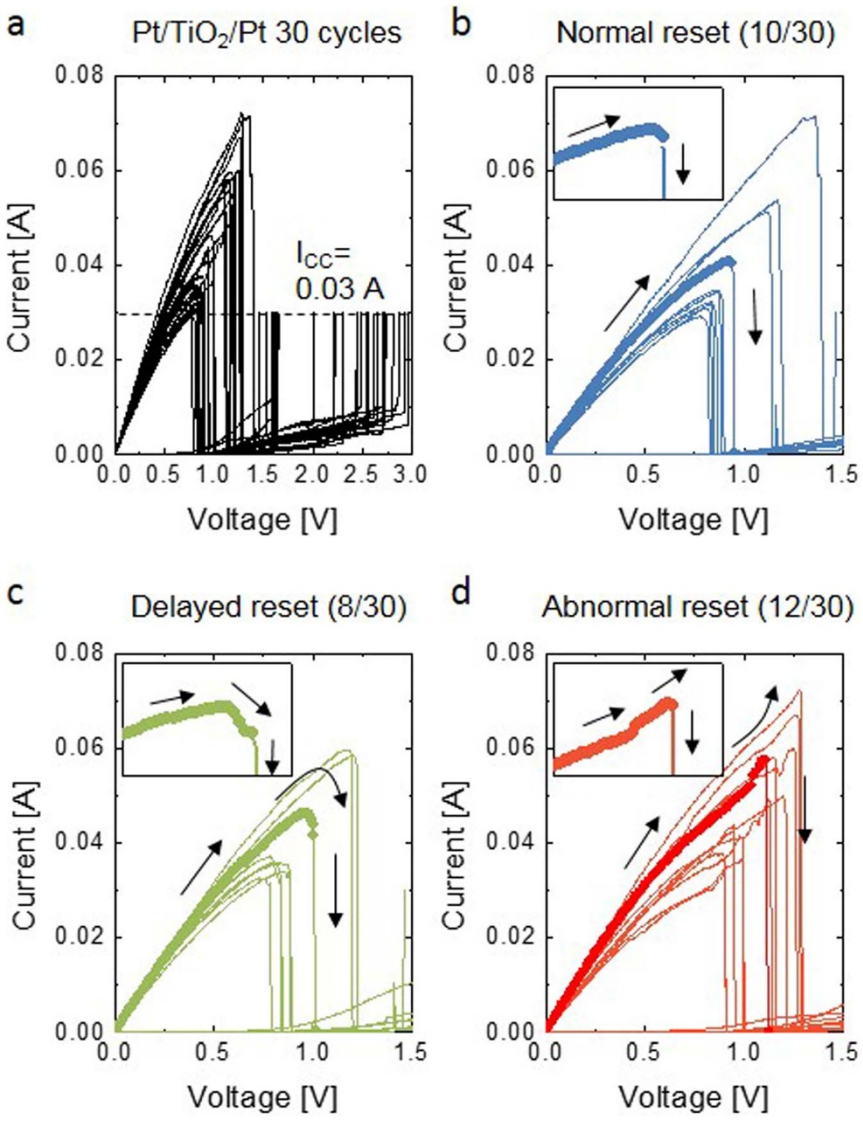

Figure 1 | The RS characteristics of Pt/TiO_2/Pt sample. (a) 30 cycles of RS I–V curves. (b) Normal reset curves, (c) delayed switching curves, and (d) abnormal reset curves were collected from (a). The insets of (b), (c), and (d) are enlarged I–V curves near the reset moment.

to the dominance of the current crowding effect for the former case, while the latter is dominated by the heat dissipation through the metal electrode with the less obvious current crowding effect[21,27]. For the reconnection by the subsequent set switching operation, the rejuvenated CF, CF_2, might have the configuration, as shown in Figure 2d. Here, the shape of the rejuvenated CF_2 might not be necessarily the same as the one before the rupture, due to the stochastic variations in the environments near CF_1, even though identical set conditions were employed during the first and second set processes. Depending on the shape of the remaining CF_1 in HRS, the rejuvenated CF_1 during the second set step may be formed either at the tip of CF_1 (more conical CF after electroforming, left side of Figure 2d) or between the two remaining parts of CF_1 (more cylindrical CF after electroforming, right side of Figure 2d).

As the set and reset switching are repeated, the filament shape will become ever more complicated. Whatever the filament shape is, however, the filaments can be divided into two parts: the retained (CF_1) and the ruptured/rejuvenated (CF_2) parts. It can be further assumed that each part has a conical shape. As the switching is repeated, further filament rupture/rejuvenation can happen either in CF_1 or CF_2, or across the two parts, which may cause the filament to be divided into three or more pieces of smaller cones. One can argue, then, that the filament shape may be too complex to be dealt with through this dual conical filament model. It does not matter, however, how complex the shape is in estimating the reset behavior using the dual conical model because the weakest part will be ruptured anyway, and the retained part can be approximated to one piece of the filament.

Based on the dual conical filament model shown in Figure 2, the filament shape can be evaluated precisely from the reset I–V curves, as follows. The first step involved calculating the thermal-resistance effect of the CF. To achieve this goal, the equilibrium temperature of the CF through Joule heating was estimated as follows. It was assumed that CF_1 and CF_2 had the cathode-side radius (the higher radius), the anode-side radius (the lower radius), and the length of r_n, $a_n \cdot r_n$, and d_n for CF_n (where n = 1, 2), respectively, as shown in Figure 2. Here it was also assumed that the distribution of oxygen vacancy is uniform along the filament so that the filament is composed of an identical Magnéli phase. Then, the resistance of a single CF_n could be calculated as $R_n = (1/a_n)(\rho \cdot d_n/\pi \cdot r_n^2)$, where ρ is the effective resistivity of the Magnéli phase ($\rho_{Ti5O7} \sim 2 \times 10^{-5}$ ohm-

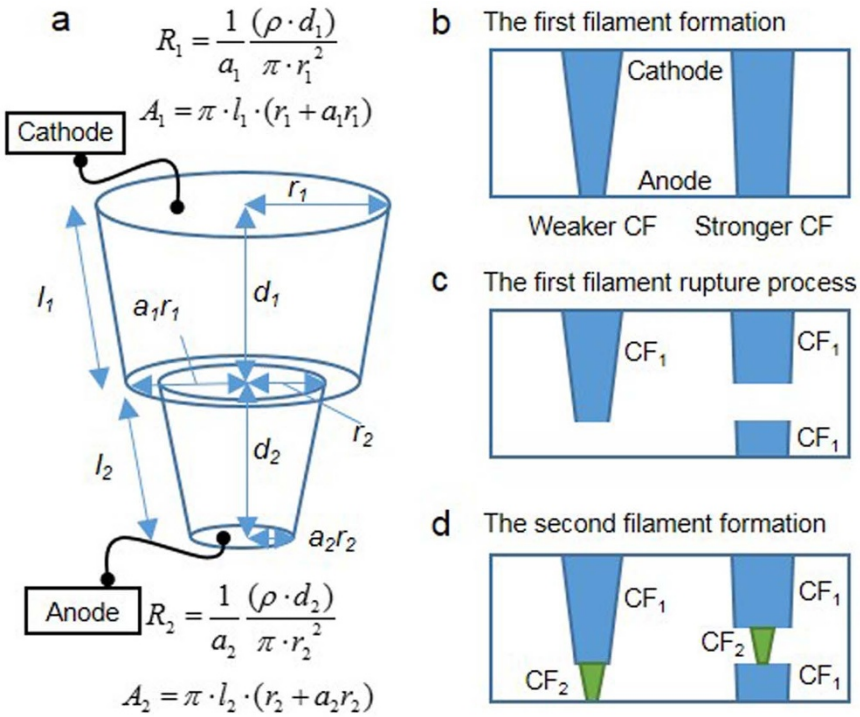

Figure 2 | The dual conical filament model. (a) The schematic diagram of the dual conical filament model in this work. (b), (c), and (d) show the filament configurations after the first filament formation (electroforming), followed the first filament rupture process (reset switching), and followed filament rejuvenation process (set switching), respectively. The left and right schematics represent a conical and a cylindrical filament, respectively.

m)[28]. Under these circumstances, the heat generation rate at CF_n could be expressed as

$$\frac{dQ_{gen,n}}{dt} = I^2 R_n = \frac{V^2}{(R_1 + R_2)^2} R_n. \quad (1)$$

In addition, the heat dissipation rate from CF_n could be expressed as

$$\frac{dQ_{dis,n}}{dt} = k \cdot A_n \cdot \frac{dT_n}{dx}, \quad (A_n = \pi \cdot l_n \cdot (r_n + a_n r_n)) \quad (2)$$

where k is the thermal conductivity of TiO_2 (k_{TiO2} = 11.7 $Wm^{-1}K^{-1}$), A_n is the surface area between one CF_n and the TiO_2 matrix, and dT_n/dx is the temperature gradient at the CF_n/matrix interface. Here, the heat transfer along the filament and the heat dissipation through the contact area with the metallic Pt electrode was not taken into account. This could cause errors in the quantitative estimation of the accurate geometry of the CFs. In fact, the heat dissipation through the metal electrode played a critical role in determining several switching parameters[29]. As will be shown later through the more complete simulation using the COMSOL package, there was indeed a certain discrepancy between the estimated geometries of the CFs when the heat dissipation was considered and when it was not considered for this analytical model. The main conclusion of this work, however, was not influenced by this discrepancy.

At the steady state, where the heat generation and dissipation rates were identical, equation (1) = equation (2). Therefore,

$$\frac{dT_n}{dx} = \frac{1}{k \cdot A_n}\frac{V^2}{(R_1 + R_2)^2} R_n. \quad (3)$$

At the small geometry near the filament boundary, dT_n/dx could be approximated to be $\Delta T_n/\Delta x$. Then, equation (3) could be

$$\Delta T_n = \frac{\Delta x}{k \cdot A_n}\frac{V^2}{(R_1 + R_2)^2} R_n. \quad (4)$$

The temperature-dependent thermal resistance could be represented as $R_n(\Delta T_n) = R_n[1 + \gamma \Delta T_n]$, where γ is the temperature coefficient of resistance (TCR). The TCR value of the Ti_nO_{2n-1} Magnéli phase is not precisely known; thus, that of Ti (γ_{Ti} = 0.0038 K^{-1}) was used for the simulation in this study[30]. This is a rather unrealistic assumption considering the very different structures of the Magnéli phase and the Ti metal. The good match, however, between the experiment and simulation results based on the proposed dual filament model shows that this is not a serious problem. In fact, many metallic conductors have similar TCR values, and a slight discrepancy in the accurate value of TCR did not influence the calculation significantly. The Δx value was set to 10 nm, which was estimated from the line of best fit of the I–V curves, as will be shown later, considering the 10–20 nm diameter of the typical Magnéli CFs. For the given γ and Δx values, the geometric parameters of the two parts of the CFs were the major variables affecting the thermal resistance of the CF, so that their changes affected the shape of the reset switching curves and the reset voltage. Therefore, the steady-state current at a given voltage V is

$$I = \frac{V}{R_1(\Delta T_1) + R_2(\Delta T_2)}. \quad (5)$$

Using the relationship between equations (4) and (5), the I–V curve of a dual filament could be obtained. Here, it should be noted that the parameters (k, γ, and Δx) used for this simulation were chosen for the best fit with the experimental results, so the precise values of them may differ from the assumed values. However, as long as the model can reproduce the experiment results well, the same conclusion can be drawn despite that there could be certain errors in

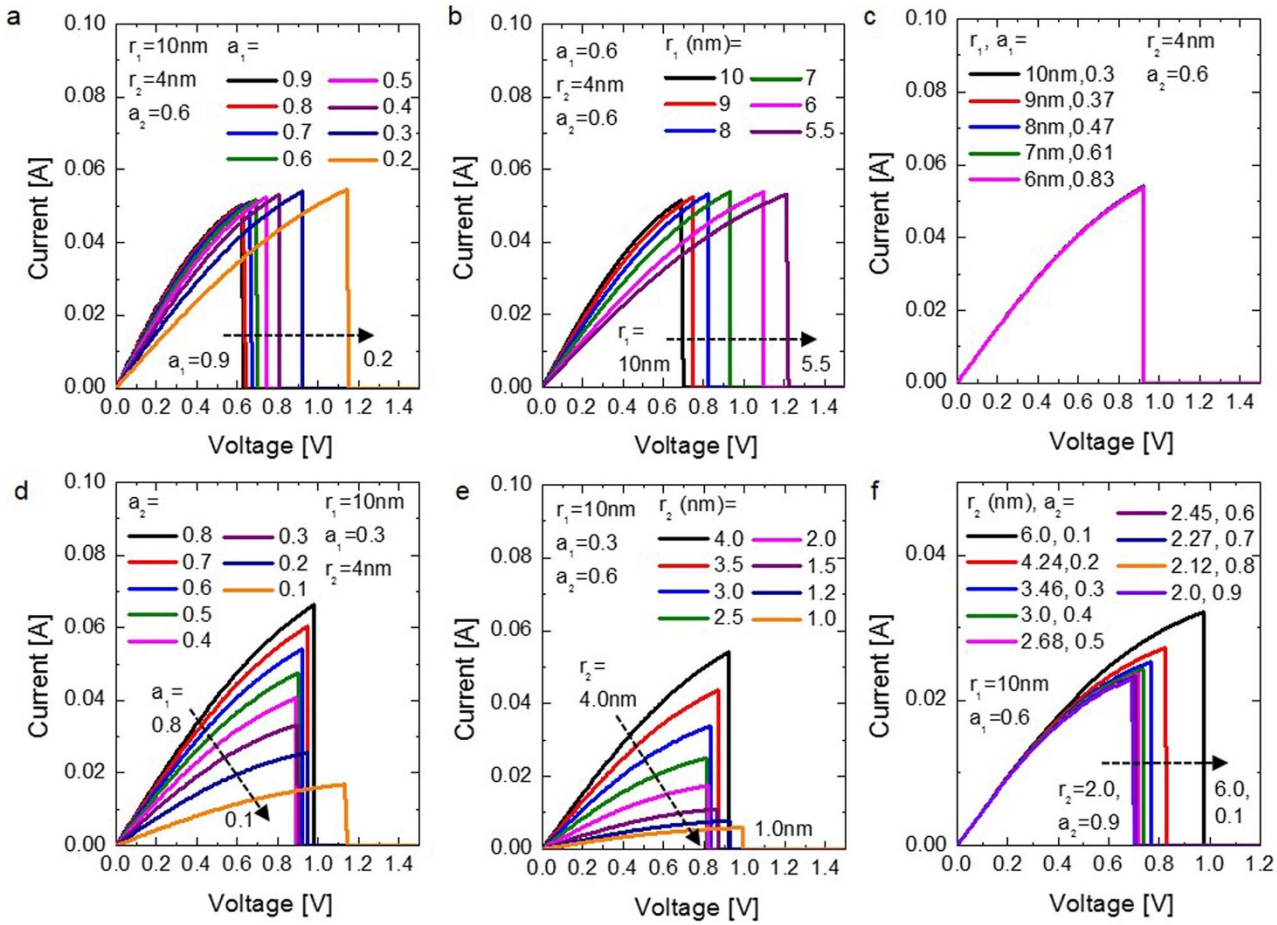

Figure 3 | The various simulated I–V curves obtained from the dual conical filament model. (a–c) show the simulated reset switching curves for the different CF_1 geometries. (a) a_1 was varied from 0.2 to 0.9 and (b) r_1 was varied from 5.5 nm to 10.0 nm for the other given parameters. (c) Both r_1 and a_1 were controlled to make the R_1 identical. (d–f) show the simulated reset switching curves for the different CF_2 geometries. (d) a_2 was varied from 0.1 to 0.8 and (b) r_2 was varied from 1.0 nm to 4.0 nm for the other given parameters. (c) Both r_2 and a_2 were controlled to make the R_2 identical.

their values. Another factor that was taken into account was the possible involvement of many parallel CFs in the I–V measurements. This was indeed the case, as shown by Choi et al.[8], using the quantitative analysis of conductive atomic force microscopy images; they reported that there are 1–2 CFs across the 500 × 500 nm^2 area in LRS, suggesting that there could be several thousands of CFs across the 100 × 100 μm^2 area in this work. The almost area-independent current values of LRS suggests that there might be local areas where the CFs present densely and sparsely, and as such, the final current values were obtained by multiplying 2,000 (2,000 parallel CFs) by the current value achieved from equation (5). In addition, the V_{RES} can be defined as the voltage where the temperature of CF_2 (ΔT_2) reaches the filament rupture temperature, which was assigned in this study as 140°C. This reset temperature was separately estimated through an experiment, where the resistance value of LRS was measured as a function of the temperature under the bias voltage of 0.2 V. For this experiment, the temperature was ramped slowly enough for the whole film temperature to be equilibrated under the weak current injection condition. It was found that the typical reset temperature was ~140–150°C. While it could be conceived that the general thermal stability of the Magnéli CFs must be quite high so that ~140–150°C may not be the temperature at which the Magnéli CFs are pure thermally ruptured, the electric-field-driven migration of oxygen ions in the region near the CFs was sufficiently activated at this temperature, and thus, reset occurred. A similar thermal resetting temperature of 110°C was also reported by Choi et al[8]. It appears that this is one of the reasons for the not sufficiently high thermal stability of LRS in TiO_2.

Figure 3 shows the various simulated I–V curves obtained from the dual conical filament model. In this simulation, the geometric parameters a_n and r_n were the main variables, and an attempt was made to determine the effect of each parameter on the reset switching curve. As can be seen in Figure 3a and b, the resetting I–V curves were calculated when a_1 and r_1, respectively, were varied for the other given parameters. That is, the influence on the reset behaviors of the change in the geometric shape of CF_1 for the given geometry of CF_2 (r_2 = 4.0 nm, a_2 = 0.6) was examined. Here, d_1 and d_2 were 30 and 10 nm, respectively, which were experimentally estimated elsewhere[11]. Certain common trends were found when the CF_1 size decreased: either r_1 or a_1 decreased, and the reset voltage increased while the reset current remained constant. As CF_1 acts as a sort of series resistor, the higher resistance of CF_1 induced a higher voltage drop on CF_1, resulting in a higher V_{RES}. This means that the actual voltage applied to CF_2 at the moment of reset must be identical irrespective of the geometry of CF_1, so that a constant amount of current for the given V_{RES} was required to rupture the CF_2, whose geometric shape was assumed to be constant. This is consistent with the report made by Kim et al., where the effect of the load resistance on the reset switching was elucidated[31]. It could be further confirmed by the simulation results shown in Figure 3c, where the $r_1 \cdot a_1$ was controlled to make the R_1 identical for the different combinations of the r_1 and a_1 values. Here, r_2 and a_2 were assumed to be 4.0 nm and

0.6, respectively. Under this circumstance, the reset switching curves for the different CF_1 geometries overlapped exactly with one another, suggesting the almost negligible role of CF_1 in varying the reset behaviors as long as CF_2 has a constant geometry. In this simulation, there could be several cases where $r_1 \cdot a_1$ is smaller than $r_2 \cdot a_2$ so that the filament rupture would likely happen at the CF_1. This corresponds to the abnormal reset case which will be discussed later. This abnormal reset showed very characteristic resetting behavior compared with other cases.

In contrast, as can be expected, the geometry of CF_2 was found to have a great influence on the reset behaviors even for the given geometry of CF_1, as shown in Figure 3d–f. In these cases, the decrease in the CF_2 size by decreasing either a_2 for the given $r_2 = 4.0$ nm and the geometry of CF_1 ($r_1 = 10$ nm, $a_1 = 0.3$) (Figure 3d), or r_2 for the given $a_2 = 0.6$ and the geometry of CF_1 ($r_1 = 10.0$ nm, $a_1 = 0.3$) (Figure 3e), drastically decreased the I_{RES}. This could be easily anticipated from the weaker strength of CF_2 for these cases. The variation in V_{RES}, however, was rather complicated despite the fact that it was lower than that of I_{RES}. This is the key element in correctly understanding the emergence of the three types of reset I–V curves shown in Figure 1, as will be discussed later. Another critical difference from the variations in the geometry of CF_2 compared with CF_1 can be found in Figure 3f, where the $r_2 \cdot a_2$ values were controlled to make the R_2 in the Ohmic region (at $V < \sim 0.3$ V) identical. In this case, as CF_2 was more cylindrical (e.g., $r_2 = 2.0$ nm, $a_2 = 0.9$), smaller V_{RES} and I_{RES} values were obtained, while the more conical CF_2 (e.g., $r_2 = 6.0$ nm, $a_2 = 0.1$) induced higher V_{RES} and I_{RES} values. This was mainly due to the larger surface area effect of the more conical filament compared to the cylindrical filament, which induced a more significant heat loss through the CF/matrix interface. These understandings of the I–V behaviors depending on the CF shape could be well utilized for understanding the three types of resetting I–V curves in the experiments shown in Figure 1.

Before the detailed discussions of the emergence of three types of reset I–V curves based on the dual conical CF model, the accuracy of the present model will be confirmed by comparing the resetting I–V curve from this relatively simple and straightforward method to the resetting I–V curve achieved using the commercial thermochemical simulation software package COMSOL, which can simulate the dynamic evolution of the temperature, electric field, and charge (current) flow across the three-dimensional volume. As the computational cost of the COMSOL simulation is quite high, only the simplest case was taken as the reference model, which is represented by Figure 4a. In figure 4b, the resulting I–V curve (green dotted line) was compared with the experiment result (black line) and with the I–V curve calculated from the analytical dual CF model (red line). For the COMSOL simulation, the sample structure was assumed to be simple metal/insulator/metal (Pt/TiO_2/Pt) fabricated on a SiO_2/Si substrate whose insulator layer had a CF structure, as shown in Figure 4a. The physical input parameters are summarized in Figure 4c, and the bias voltage was applied to the top electrode while the bottom electrode was grounded. Due to the very different electrical conductivities of TiO_2 and Magnéli CFs, almost all the current flowed only through the CFs, which induced the local Joule heating effect, as shown by the color code in Figure 4a. There could be multiple CFs connecting the top and bottom electrodes, however, which was indeed the case in the experiment[8], and as such, it was assumed that the electricity was conducted through 2,000 parallel CFs. Due to this parallel configuration of the CFs, the calculated current though one CF was multiplied by 2,000 to finally obtain the I–V curve. In this COMSOL simulation, it must be noted that the heat loss through the contacting electrodes were also taken into account. The input geometric parameters for the CFs in the COMSOL and dual CF simulations are summarized in Figure 4d. It could be immediately understood that both simulations precisely reproduced the experimental I–V curve using the assumed geometric

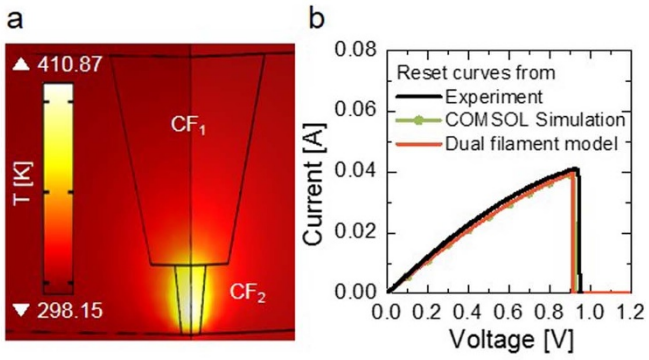

c

	Thermal conductivity (W/m·K)	Density (kg/m^3)	Heat capacity (J/kg·K)	Electrical conductivity (S/m)
Si	131	2329	700	1
SiO_2	1.4	2200	730	1.0×10^{-6}
Pt	71.6	21450	133	8.9×10^{6}
TiO_2	6	4150	711	1.5×10^{-8}
Magnéli phase (filament)	9	4180	693	$\rho(\Delta T)=\rho_0(1+\gamma\Delta T)$ $\rho_0=2\times10^{-5}$ (Ω·m) $\gamma=0.0038$(1/K)

d

	COMSOL	Dual CF
CF_1	r_1=15nm, a_1=0.2, d_1=30nm	r_1=6nm, a_1=0.9, d_1=30nm
CF_2	r_2=3nm, a_2=0.6, d_2=10nm	r_2=3nm, a_2=0.6, d_2=10nm

Figure 4 | The comparison of the thermochemical simulation by COMSOL and the dual conical filament model. (a) COMSOL simulation result for the simplest dual conical filament. (b) The resulting COMSOL simulation I–V curve (green dotted line) was compared with the experiment result (black line) and with the I–V curve calculated from the analytical dual CF model (red line). (c) The physical input parameters used for the COMSOL simulation. (d) The input geometric parameters for the CFs in the COMSOL and dual CF simulations.

parameters. Therefore, the validity of the much simpler dual CF model could be confirmed from these comparisons, despite its simpler formalism and much lower computational cost. Nevertheless, there are certain discrepancies among the assumed geometric parameters to achieve a good coincidence between the two different simulations. This is explained further below. For both simulations, there are six geometric variables, which made the fitting highly arbitrary. As aforementioned, however, d_1 and d_2 could be reasonably assigned the values of 30 and 10 nm, respectively, from the experiment. Then, there are four remaining variables (r_1, a_1, r_2, and a_2) to be determined. For the dual CF model, which takes almost a negligible time to perform the calculation, the four variables were varied within certain ranges, considering the trend shown in Figure 3, and it was finally figured out after many trials that the geometric parameters shown in Figure 4d are the appropriate values. There could be several other combinations, but for the given constraints of $r_1 > r_2$, no other combination produced such a good coincidence with the experiment results. In the course of such trials, it was found that the I–V curve shape was more dependent on the geometry of CF_2 than on that of CF_1, which is certainly understandable considering the much higher resistance of CF_2 compared with CF_1. Therefore, the geometric para-

meters for CF_2 were retained as they were identical to those of the dual CF simulation in the case of the COMSOL simulation. When the geometric parameters for CF_1 were also retained, however, the current level was generally too low for the whole voltage region, so that the geometry of CF_1 must be assumed to be more conical (r_1 = 15 nm, a_1 = 0.2) for the COMSOL simulation. Such discrepancy must have a close relationship with the conceived heat loss via the electrodes in the COMSOL case, but more detailed discussions of such will be given in another publication because this is beyond the scope of this work.

Another very interesting finding was that the maximum temperature that CF_2 encountered at the moment of reset (V-0.9 V) was ~411 K, which was very close to the assumed reset temperature of 140°C in the dual CF simulation. This again confirmed the usefulness and accuracy of the dual CF model despite its simple and easy calculation. It appears that the weakness of not considering the heat loss through the electrodes was compensated for by the slightly modified geometry of CF_1 (slightly more cylindrical) compared with the actual more conical shape. Below, detailed discussions of the reasons for the emergence of three types of resetting curves are provided based on the understanding that could be achieved by using the dual CF model.

The occurrence of the normal reset curve was well explained from the aforementioned mutually constructive interference between the Joule heating and temperature-dependent resistance effects of the metallic CF. This could be slightly more precisely understood from the variations in V_{RES} with the decreasing r_2 or a_2 in Figure 3d and e. When a_2 decreased from 0.8 to 0.4, as shown in Figure 3d, and when r_2 decreased from 4.0 to 2.5 nm, as shown in Figure 3e, which corresponded to the filament size decrease, V_{RES} decreased. This implies that the reset process can be "self-activated" once the reset switching is initiated (i.e., when the CF_2 size starts to decrease).

For the delayed reset, the following can be considered. The delayed reset can be characterized as the relatively slow transition to HRS near the current peak, which can be simulated by the I–V curves included in Figure 5. Here, the main variable was a_2, which varied from 0.26 to 0.20 for the other given geometric parameters (r_2 = 4.6 nm, a_1 = 0.8, and r_1 = 8.0 nm). One of the experimental delayed reset I–V curves is represented by the red-circle symbols. The experimental I–V curve could be very well fitted using the reset behavior of a certain CF with an a_2 value of 0.26 up to the voltage where the current started to decrease (~0.78 V). The gradual decrease in the current within the voltage region from ~0.78 to ~0.83, however, could not be fitted by any single set of variables. The only feasible fitting results could be achieved by introducing the change in a_2. The inset in Figure 5 shows an enlarged portion near the current peak, showing a good fit with the experiment data. It has to be noted that the current at the voltages well below the V_{RES} could be fitted only with a_2 = 0.26, suggesting that the change in the CF_2 shape occurs only when the CF_2 tip is heated sufficiently, up to near the rupture temperature, so that CF_2 has started to be varied. This means that the CF_2 shape (not just the size with a constant shape) can change during the resetting process, which is most likely the case when the CF_2 has a more conical shape (small a_2) and a smaller size (r_2). This corresponds to the a_2 range from 0.4 to 0.1 in Figure 3d, and the r_2 range from 2.5 to 1.0 nm in Figure 3e, respectively. In this regime, a partial rupture of the filament causes an increase of the V_{RES} so that the reset switching is no longer instantaneous.

Explaining the abnormal reset behavior shown in Figure 1d using a similar I–V simulation is slightly trickier, but this can be well performed when the configuration of CF is assumed to be the one shown in Figure 6. The obvious difference between the I–V curves shown in Figure 6 and those in Figure 5 is the deviation into a higher current value immediately prior to the reset switching from the simulating I–V curve assuming a single set of simulation parameters in the low-voltage region. Such variation could not be simulated by any combination of the parameters for only CF_1 or CF_2 (r_1, a_1 or r_2, a_2), which suggests that the parameters for both portions of the CF must vary simultaneously. Among the four variables, (r_1, a_1, r_2, a_2), r_1, and r_2 are the most unlikely to vary because these parameters represent the most stable parts of the two portions (the largest-diameter parts of the two portions). Therefore, the two other parameters (a_1 and a_2) were taken as the relevant variables, and one of the representative experimental I–V curves was attempted to be fitted, as shown in Figure 6a, which shows a quite good coincidence between the experiment and simulation results. The top inset in Figure 6a shows the enlarged portion near the current peak. For this fitting, a_1 and a_2 must be taken as shown in Figure 6b. As a result of varying a_1 and a_2 for the given r_1 and r_2 of 6.3 and 4.8 nm, respectively, the R_1 and R_2 and their sum (R_1 + R_2) varied, as shown in Figure 6c. No other combination of variables could have resulted in such a good fit. Such variations in R_1 and R_2 (and thus, in a_1 and a_2) indicate that the CF configuration varies in the following manner immediately prior to the reset occurrence. The increasing R_1 can be interpreted as indicating that the diameter near the CF_1 tip is decreasing (decreasing a_1), which is quite normal for a reset to occur. The decreasing R_2 suggests, however, that CF_2 actually becomes stronger immediately prior to the reset, which is quite abnormal from the usual consideration. From the generally high I_{RES} trend in Figure 1d of this case compared with other cases, it can be conjectured that the overall shape of the CF after the set could be more cylindrical, so that the subsequent reset, set, and final reset switching may proceed as shown in the sequence indicated in the right schematic diagrams in Figure 2b–d. The details of this peculiar reset process can be explained by the schematic diagrams shown in Figure 6d. When the cylindrical filament is ruptured at the middle portion, followed by its rejuvenation, a step can be formed at the boundary between the tip of the rejuvenated portion of the filament (CF_2) and the top of the remaining anode-side original filament (CF_1) (bottom inset in Figure 6a). When the overall CF was heated during the reset process, the oxygen near the CF/matrix interface could move, as shown in Figure 6d. This resulted in the weakening and strengthening of the weaker parts of CF_1 and CF_2, as shown in the right schematic diagram in Figure 6d, which was consistent with the assumed variations in R_1 and R_2 (thus, a_1 and a_2) in Figure 6c. Once the overall shape of

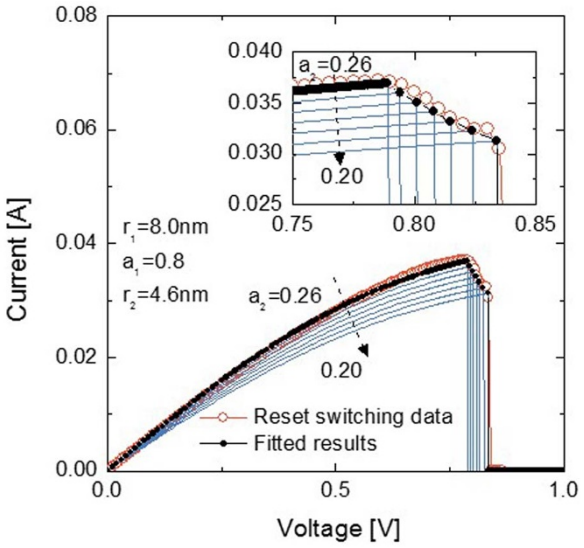

Figure 5 | The dual conical filament model for the delayed reset case. One of the experimental delayed reset I–V curves is represented by the red-circle symbols. The simulated I–V curves with a_2 values from 0.26 to 0.20 are represented by the blue lines. The inset shows the enlarged I–V curves near the reset moment.

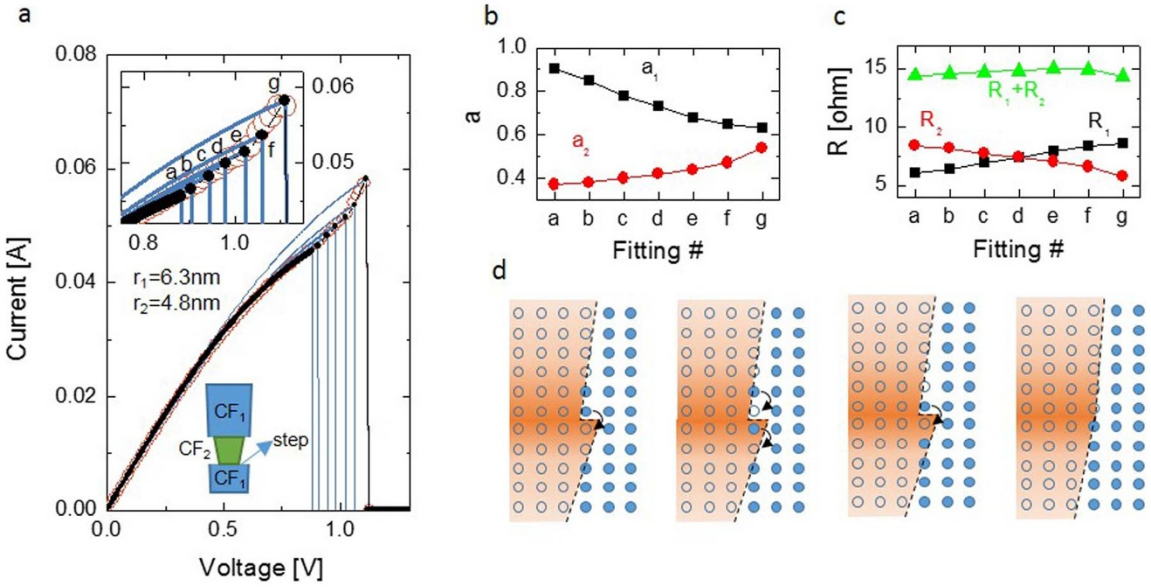

Figure 6 | The dual conical filament model for the abnormal reset case. (a) One of the experimental abnormal reset I–V curves is represented by the red-circle symbols. The simulated I–V curves are represented by the blue lines. The top inset shows the enlarged I–V curves near the reset moment. The bottom inset shows the schematic dual filament configuration for the abnormal reset. (b) The fitting values of a_1 and a_2 used for the simulation. (c) Variation of R_1, R_2 and $R_1 + R_2$ in accordance with the variation of (b). (d) The schematic diagrams of the filament evolution process when the filament has a kink/step geometry.

CF becomes almost flat and conical through the repetition of the oxygen atom migration/diffusion process shown in Figure 6d, the CF_2 is merged into CF_1 and the bottom part of CF_1 is changed to a new CF_2, then the normal reset will finally occur near the weakest tip of the final CF structure. Therefore, the abnormal reset process can be understood quantitatively based on the reset process represented by Figure 6d.

In conclusion, the dual conical filament model was suggested to explain the disparate resetting I–V curves of the Pt/TiO_2/Pt RS cells, which could be grouped into three types; normal, delayed, and abnormal behaviors. The fundamental idea was based on the two previous understandings in the field: that there must be a remaining CF portion near the cathode interface, which is quite unaltered even after the reset, and that the overall CF shape could be more conical or cylindrical depending on the CF strength. The stochastic nature of the set processes during the repeated RS via the I–V sweeps could result in all the three types of reset behavior. The three distinctive resetting behaviors could be well simulated by assuming the variations in the different portions of the CFs depending on their detailed shapes, which were determined during the previous set step. The almost spontaneous resetting behavior of the normal reset could be easily understood from the mutually constructive interference effect between the Joule heating and temperature-dependent resistance effect along the CF. The delayed and abnormal resetting behaviors, however, required specific CF models, whose detailed variations were dependent on the dynamic evolution of the weakest part of the CF with time. The delayed reset could be explained by the time-dependent increase in the V_{RES} during the rest process, which was most probably induced in a more conical-shaped CF. The abnormal reset could be understood from the temporal transfer of oxygen ions near the kink positions of the two different-diameter portions of the more cylindrical CFs, which temporally decreases the overall resistance immediately prior the actual reset occurrence. Such an understanding of the detailed processes involved in the reset process could be a great help in improving the switching uniformity and controllability of the RS, e. g. forming a strong CF_1 by using a higher compliance current and then performing the RS of CF_2 using a smaller compliance current to confine the filament rupture location within CF_2. More detailed experimental results will be reported elsewhere.

1. Lee, M.-J. *et al.* A fast, high-endurance and scalable non-volatile memory device made from asymmetric Ta2O(5-x)/TaO(2-x) bilayer structures. *Nat. Mater.* **10**, 625–30 (2011).
2. Strukov, D. B., Snider, G. S., Stewart, D. R. & Williams, R. S. The missing memristor found. *Nature* **453**, 80–3 (2008).
3. Jo, S. H. *et al.* Nanoscale memristor device as synapse in neuromorphic systems. *Nano Lett.* **10**, 1297–301 (2010).
4. Waser, R., Dittmann, R., Staikov, G. & Szot, K. Redox-Based Resistive Switching Memories - Nanoionic Mechanisms, Prospects, and Challenges. *Adv. Mater.* **21**, 2632–2663 (2009).
5. Kim, K. M., Jeong, D. S. & Hwang, C. S. Nanofilamentary resistive switching in binary oxide system; a review on the present status and outlook. *Nanotechnology* **22**, 254002 (2011).
6. Jeong, D. S. *et al.* Emerging memories: resistive switching mechanisms and current status. *Rep. Prog. Phys.* **75**, 076502 (2012).
7. Rohde, C. *et al.* Identification of a determining parameter for resistive switching of TiO_2 thin films. *Appl. Phys. Lett.* **86**, 262907 (2005).
8. Choi, B. J. *et al.* Resistive switching mechanism of TiO_2 thin films grown by atomic-layer deposition. *J. Appl. Phys.* **98**, 033715 (2005).
9. Kim, K. M. *et al.* Resistive Switching in Pt/Al_2O_3/TiO_2/Ru Stacked Structures. *Electrochem. Solid-State Lett.* **9**, G343 (2006).
10. Kim, K. M., Choi, B. J. & Hwang, C. S. Localized switching mechanism in resistive switching of atomic-layer-deposited TiO_2 thin films. *Appl. Phys. Lett.* **90**, 242906 (2007).
11. Kim, K. M., Choi, B. J., Shin, Y. C., Choi, S. & Hwang, C. S. Anode-interface localized filamentary mechanism in resistive switching of TiO_2 thin films. *Appl. Phys. Lett.* **91**, 012907 (2007).
12. Kim, K. M. & Hwang, C. S. The conical shape filament growth model in unipolar resistance switching of TiO_2 thin film. *Appl. Phys. Lett.* **94**, 122109 (2009).
13. Kwon, D.-H. *et al.* Atomic structure of conducting nanofilaments in TiO_2 resistive switching memory. *Nat. Nanotechnol.* **5**, 148–53 (2010).
14. Song, S. J. *et al.* Real-time identification of the evolution of conducting nano-filaments in TiO_2 thin film ReRAM. *Sci. Rep.* **3**, 3443 (2013).
15. Hwan Kim, G. *et al.* Improved endurance of resistive switching TiO_2 thin film by hourglass shaped Magnéli filaments. *Appl. Phys. Lett.* **98**, 262901 (2011).
16. Kim, K. M. *et al.* Collective Motion of Conducting Filaments in Pt/n-Type TiO_2/p-Type NiO/Pt Stacked Resistance Switching Memory. *Adv. Funct. Mater.* **21**, 1587–1592 (2011).
17. Jeong, D. S., Schroeder, H. & Waser, R. Coexistence of Bipolar and Unipolar Resistive Switching Behaviors in a Pt/TiO_2/Pt Stack. *Electrochem. Solid-State Lett.* **10**, G51 (2007).

18. Yoon, K. J. *et al.* Evolution of the shape of the conducting channel in complementary resistive switching transition metal oxides. *Nanoscale* **6**, 2161–9 (2014).
19. Kim, K. M. *et al.* A detailed understanding of the electronic bipolar resistance switching behavior in Pt/TiO_2/Pt structure. *Nanotechnology* **22**, 254010 (2011).
20. Kim, K. M., Han, S. & Hwang, C. S. Electronic bipolar resistance switching in an anti-serially connected Pt/TiO_2/Pt structure for improved reliability. *Nanotechnology* **23**, 035201 (2012).
21. Kim, K. M. *et al.* Electrically configurable electroforming and bipolar resistive switching in Pt/TiO_2/Pt structures. *Nanotechnology* **21**, 305203 (2010).
22. Song, S. J. *et al.* Identification of the controlling parameter for the set-state resistance of a TiO_2 resistive switching cell. *Appl. Phys. Lett.* **96**, 112904 (2010).
23. Kim, K. M. *et al.* Understanding structure-property relationship of resistive switching oxide thin films using a conical filament model. *Appl. Phys. Lett.* **97**, 162912 (2010).
24. Lee, S. B., Chae, S. C., Chang, S. H. & Noh, T. W. Predictability of reset switching voltages in unipolar resistance switching. *Appl. Phys. Lett.* **94**, 173504 (2009).
25. Kim, K. M. *et al.* Methods of Set Switching for Improving the Uniformity of Filament Formation in the TiO_2 Thin Film. *Electrochem. Solid-State Lett.* **13**, G51 (2010).
26. Yoon, J. H. *et al.* Role of Ru nano-dots embedded in TiO_2 thin films for improving the resistive switching behavior. *Appl. Phys. Lett.* **97**, 232904 (2010).
27. Russo, U. *et al.* Self-Accelerated Thermal Dissolution Model for Reset Programming in Unipolar Resistive-Switching Memory (RRAM) Devices. **56**, 193–200 (2009).
28. Bartholomew, R. & Frankl, D. Electrical properties of some titanium oxides. *Phys. Rev.* **187**, 828–833 (1969).
29. Chang, S. H. *et al.* Effects of heat dissipation on unipolar resistance switching in Pt/NiO/Pt capacitors. *Appl. Phys. Lett.* **92**, 183507 (2008).
30. Gale, W. & Totemeier, T. *Smithells metals reference book* (Elsevier Butterworth-Heinemann, 2003).
31. Kim, G. H. *et al.* Influence of the Interconnection Line Resistance and Performance of a Resistive Cross Bar Array Memory. *J. Electrochem. Soc.* **157**, G211 (2010).

Acknowledgments

C.S. Hwang acknowledges the support of the Global Research Laboratory Program (2012040157) through the National Research Foundation (NRF) of South Korea.

Author contributions

K.M.K. designed and performed the experiment and the dual conical filament simulation, and wrote the manuscript. T.H.P. performed the COMSOL simulation, and C.S.H. arranged and supervised all the experiments and took charge of the manuscript preparation. All the authors reviewed the manuscript.

Additional information

Competing financial interests: The authors declare no competing financial interests.

How to cite this article: Kim, K.M., Park, T.H. & Hwang, C.S. Dual Conical Conducting Filament Model in Resistance Switching TiO_2 Thin Films. *Sci. Rep.* **5**, 7844; DOI:10.1038/srep07844 (2015).